Superflexibility of ITO Electrodes via Submicron Patterning

Qian Dong,[†] Yukihiro Hara,[‡] Kristina T. Vrouwenvelder,[§] Kai T. Shin,[†] Jared A. Compiano,[‡] Mohtashim Saif,[∥] and Rene Lopez*[,‡]

[†]Department of Applied Physical Sciences, [‡]Department of Physics and Astronomy, and [§]Department of Chemistry, University of North Carolina at Chapel Hill, Chapel Hill, North Carolina 27599, United States

[∥]Eastman Chemical Company, Canoga Park, California 91304, United States

ABSTRACT: Indium tin oxide (ITO) is the premier choice for transparent conductive electrodes in optoelectronic devices despite its inherent brittleness. Here we report the fabrication of a grating-like structure that obviates ITO's mechanical limitations while retaining its resistivity and optical qualities. ITO nanopatterned films exhibited a resistivity $<1.3 \times 10^{-3}$ Ω cm, which surpassed all previously reported values for flexible ITO, with a normal transmission >90% across the whole visible spectrum range. We demonstrate the nanopatterned ITO retains extraordinary flexibility and durability on heat-sensitive substrates, accommodating cyclic bending to a curvature diameter of at least 3.2 mm for over 50 cycles of compressive and decompressive flexing without significant deterioration of its resistivity or optical properties. Moreover, 2-dimensional extrapolation shows that multiaxial bending is also feasible while maintaining mechanical flexibility, durability, and optical transparency.

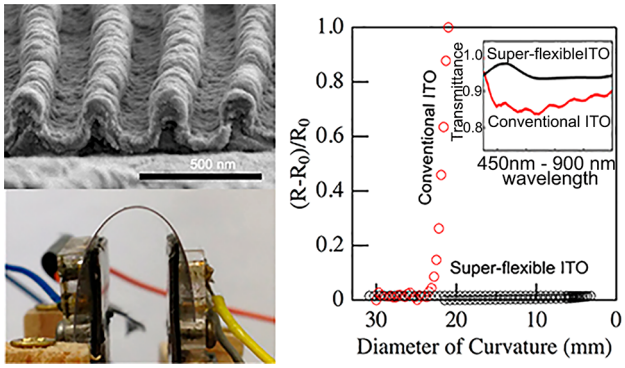

KEYWORDS: *transparent electrodes, indium tin oxide, periodic grating pattern, flexibility, transmittance*

1. INTRODUCTION

Clear substrates coated with indium tin oxide (ITO) thin films are ubiquitous as transparent conductive electrodes in liquid crystal displays (LCDs),[1,2] organic light-emitting diodes (OLEDs),[3−6] touch screens, thin-film transistors (TFTs),[7,8] solar cells,[9,10] e-paper, and sensors.[11] For several decades ITO and other transparent conductive oxides have fulfilled device performance requirements in terms of transparency and conductivity. Now ITO films face an important challenge: the technological push toward flexible devices requires transparent electrodes on highly flexible and heat-sensitive polymer substrates. As with all oxide ceramics, ITO's inherent brittleness is a serious disadvantage for its incorporation in highly flexible electronics, since cracking and/or delamination will adversely impact the performance and lifetime of devices. Moreover, the high refractive index of ITO with its associated optical effects when deposited on polymer substrate cannot be ignored when employed in image display-related devices: In the visible spectrum the refractive index of ITO is approximately 2.0, which gives rise to a strong reflection and diminished optical transparency for incident light on ITO-coated polymer substrates.[12,13]

In order to overcome these challenges, researchers have considered radically different material alternatives for flexible transparent contacts such as single-walled carbon nanotubes (CNTs),[14−17] graphene,[18−20] metal nanopatterns[21] or metal nanowires (NW),[12,22−24] and hybrids of these.[25−27] While these materials have exhibited good durability when they were subjected to external mechanical stresses, there is an unavoidable compromise: the trade-off between high electrical conductivity and optical transparency. And to improve the resistance of a layer, a thicker film is needed, and this, in turn, lowers the transparency.

Therefore, ITO remains the industry's material of choice,[12] and investigations on how to improve its mechanical properties have been focused on alternative ITO morphologies. ITO with nanoporous and nanoarray-based structures have attracted attention because of the relative independence of its conductivity and transparency. For ITO porous coatings, the most successful approach derives from depositing nanoparticles from solution to form a porous structure that effectively improves its optical transparency. But this methodology requires relatively high sintering temperatures to build up the interconnections between nanoparticles and achieve competitive levels of electrical conductivity. This high temperature step is an obstacle for heat-sensitive polymer substrates typically utilized in flexible optoelectronic devices. Approaches aimed at lowering the sintering temperature have been advanced in

Received: December 15, 2017
Accepted: March 6, 2018
Published: March 6, 2018

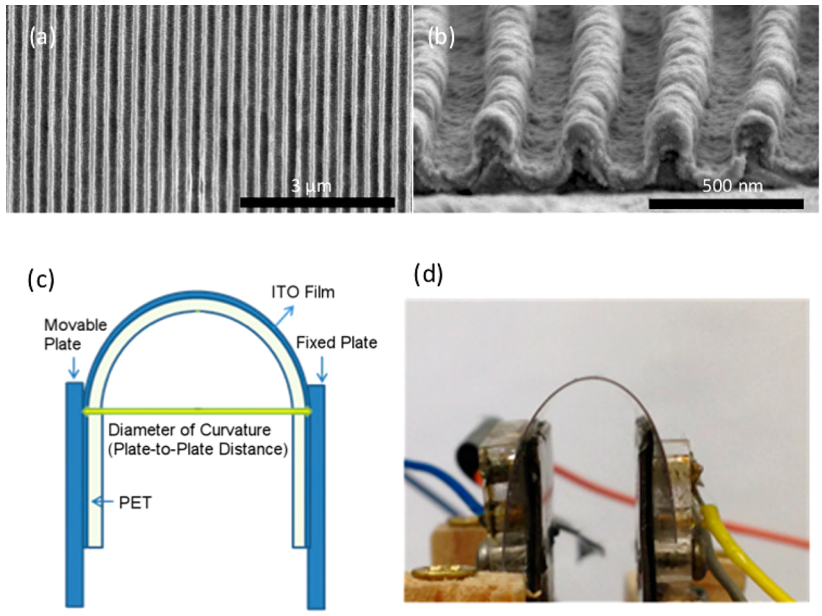

Figure 1. SEM surface image (a) and cross-section image (b) of the morphology of the ITO periodic grating patterns on the surfaces of the polymer substrates. (c) and (d) illustrate the schematic diagram and corresponding photograph of the bending system, respectively. Notice the film convex location relative to the substrate upon bending.

recent years.[28−32] Maksimenko et al., for instance, reported the fabrication of porous ITO coatings via a solution-based process with a relatively low sintering temperature of 130 °C.[31,32] A resistivity in the range of 10^{-1} Ω cm (with a sheet resistance of >400 Ω sq^{-1}) and an optical transparency of 85−90% were achieved. Yun et al. successfully deposited an ITO nanoarray on flexible heat-sensitive polyethylene terephthalate (PET) substrates at room temperature with further improvement in both electrical conductivity and optical transparency (a resistivity of approximately 2.3 × 10^{-3} Ω cm and a local transmission of about 99% at 550 nm).[33] Although these films demonstrated some improvement in their mechanical flexibility, they all failed catastrophically on reaching a bending curvature <8 mm diameter. In summary, substantially better ITO mechanical flexibility together with smaller decrements in electrical and optical properties constitutes a technologically important goal to enable the utilization of transparent electrodes on heat-sensitive, soft polymer substrates.

In this paper, we report on several advancements in developing a flexible transparent ITO conductive electrode on PET based on a spring architecture. Spring-like structures are a well-known mechanical solution for extension and contraction with minimum stress/strain. Thus, it is not surprising that such solution can be considered as a promising architecture for flexible electronic devices. Indeed, this approach has been proven to add flexibility to important electronic brittle materials such as silicon.[34] Employing laser interference lithography, we initially fabricated a 1-dimensional (1-D) submicron grating structure to serve as the ITO-PET interface. Subsequently, a uniform ITO film was deposited on the nanopatterned structure at room temperature by conventional commercial sputtering deposition. The ITO microstructured film showed superior flexibility and durability than its nonpatterned counterparts as well as other reported ITO flexibility-improved films. The bending diameter of curvature of the films was successfully tested down to 3.2 mm without cracking. (This curvature target was suggested by our commercial ITO producing partners, and it is the smallest we could test with our bending apparatus.) Multiple samples were fabricated and evaluated with all of them showing, after 50 cycles of bending, relative electrical resistance changes within 20% and in most cases below 3%. (For reference, a standard flat film resistance increases >100 times with a single bending cycle in this bending curvature.) To expand its potential commercial applicability, this enhanced flexibility is also demonstrated in a 2-dimensional (2D) fashion, with resistance changes still below 50% after 50 cycles of bending over two perpendicular axes. All samples were subjected to multiple cycles of compression and decompression and maintained commercially required levels of electrical resistance and optical transparency. More importantly, with each bending cycle, the resistance changes got smaller.

2. EXPERIMENTAL SECTION

Materials. 1 × 1 $in.^2$ (25.4 × 25.4 mm^2) PET films with a thickness of 125 μm were used as the substrates in this study. PET sheets were purchased from TAP Plastics Inc. MCC Primer, S1811 positive photoresist, Thinner-P, and MF 319 developer were purchased from Microchem.

Fabrication of ITO Submicron Patterning. The substrate patterning and ITO deposition proceeded over two simple, already commercially employed steps (Figure S1 in Supporting Information): (1) fabrication of the submicron structure with a photoresist and (2) deposition of ITO onto the photoresist structure via sputtering. Since the spring-like structure needs to be transparent in the whole visible range, it must be fabricated with sub-optical wavelength dimensions to avoid angular diffractive effects. Maskless laser interference lithography (LIL) allows a fast and large area of periodical structures to be patterned with simple equipment[35] at great speed (a few seconds to few minutes depending on laser fluence, without the need of precision sample placement). Adequate periodicity and the height of the spring-like structure were chosen by diffractive optics modeling and fabricated by controlling the exposure dose and angles between the two interference beams.[36]

The LIL process was carried out on positive photoresist S1811. In order to produce the structure with a specific height (180 nm in this study), the dilute photoresist solution was used, in which the ratio of pure photoresist to Thinner-P was 1:1 and 1:2 in volume, respectively.

The photoresist solution was spin-coated at 7000 rpm for 40 s onto a PET substrate and followed by prebaking on the hot plate at 120 °C for 60 s. The photoresist-coated film was then mounted in the interference lithography setup and exposed to the UV laser with 405 nm wavelength for 4 min. After exposure, the substrate was dipped into MF 319 developer for 7 s right away, followed by washing step with deionized water, in which the substrate was rinsed for 7 s twice. After that, the substrate was dried with the N_2 flow. ITO was then deposited on the periodic grating pattern template comprised of a photoresist on PET by roll-to-roll sputtering deposition at room temperature.

Characterization. The cross-sectional images of ITO periodic submicron grating structure were obtained using a scanning electron microscopy (SEM, Hitachi S-4700). The specimens were cross-sectioned in liquid nitrogen in order to minimize the tearing damage to the polymer substrate during the cutting process. The transmittance of ITO nanopatterned PET substrates was measured with an integrating sphere and spectrometer/CCD camera (Acton 300, PIXIS, Princeton Instruments).

The initial sheet resistance of ITO periodic submicron grating structure was determined by the mean value of at least three different measurements with the same condition by using a four-point probe system (Signatone1160 series probe station). The mechanical flexibility of ITO nanopatterned PET substrates was then measured with a lab-made bending system composed of two parallel plates with a programmable separation distance. During the forward and backward bending process, the electrical sheet resistance of the specimen was measured by four-point measurement via a NI-4065 multimeter as a function of bending diameter of curvature, which was the distance between the two plates of the bending system. During the bending test, the sample was bent into given diameters of curvature in discrete small steps. At each diameter of curvature, the movement was paused to measure via four-point probe the sheet resistance. The probes were spring set on the four corners of the square-shaped samples, relatively far from the strained region. Each bending cycle included compressing and decompressing steps. The test specimens were subjected to 50 bending cycles with the minimum bending diameter of curvature being 3.2 mm, that as mentioned earlier was limited by the apparatus range.

3. RESULTS AND DISCUSSION

In our first realization of the structure, the ITO grating had a 285 nm periodicity and a total height of 230 nm (which includes the grating height of photoresist and the thickness of ITO layer). Figures 1a and 1b show the surface and cross-sectional micrographs of the ITO periodic submicron grating structure deposited on the PET substrates. As can be noted in the micrograph, the deposition of ITO on the grating template is quite uniform. Even though the aspect ratio (height/pitch) of the structure was ~0.9, the peaks and valleys of the grating were coated only slightly thinner than the control flat ITO layer. The measured sheet resistance of all the ITO films on patterned PET substrates fabricated via the same conditions were approximately the same, with a deviation of 5%. The lowest sheet resistance observed was 209 Ω sq^{-1}, which corresponded to a resistivity of 1.4×10^{-3} Ω cm. (This was calculated from the sheet resistance using the thickness of the ITO layer ~67 nm.) Compared to the resistivity values previously reported for porous ITO films via solution-based process[31,32] and ITO nanoarray via sputtering-based process,[33] the sheet resistance of the ITO nanopatterned films analyzed in this study was at least 20% better. Relative to the control flat samples though, the electrical sheet resistance of the patterned specimens was approximately 10% higher. Taking the grating aspect ratio into account, this difference is understandable since the conductive path of ITO patterned structure was longer and its thickness was slightly thinner at the pattern walls than that of the flat sample; the introduced geometrical change must indeed induce a slightly higher sheet resistance.

The mechanical flexibility and durability of the ITO periodic submicron grating structures were tested by applying a high tensile or compressive stress to the ITO nanopattern via bending as illustrated in Figure 1c,d. Figures 2a and 2b show

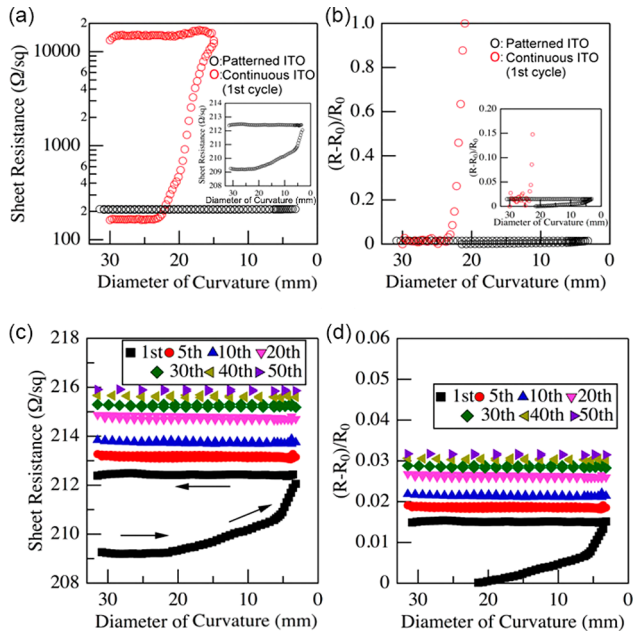

Figure 2. Comparison of the sheet resistance (a) and relative resistance increase (b) between ITO periodic grating patterns and continuous films on the surfaces of the polymer substrates as a function of diameter of curvature during the bending test. Insets show the magnified scale. Notice the film convex location relative to the substrate upon bending. The (c) sheet resistance and (d) relative resistance increase of the ITO periodic grating patterns on the surfaces of the polymer substrates during the cycling bending test. During each cycle, the minimum bending diameter of curvature was kept at 3.2 mm, and the specimen experienced 50 cycles of the reversible bending test.

the sheet resistance and the resistance change upon bending the first cycle for the flat control and the patterned 285 nm pitch ITO samples, respectively. The contrast can hardly be more dramatic; when the curvature diameter has decreased to barely 23.5 mm, the sheet resistance of flat ITO film has already undergone a very large 100-fold resistance increase. The post-test examination of this conventional ITO film under electron microscope showed that large cracks and some delamination (Figure S2 in Supporting Information) were responsible for the deteriorated resistance, leading to an irreversible catastrophic failure. In contrast, the ITO patterned sample stayed approximately the same all the way to the smallest possible bending in the instrument without any obvious structural change (Figure S3). The relative resistance change for the patterned ITO film was less than 1.6% after the first bending cycle.

Remarkably, with <2% resistance deterioration, this first bending cycle is the biggest single damaging event the films patterned with this nanostructure will suffer if continue evaluating over multiple consecutive bending tests. Figures 2c and 2d show the sheet resistance and relative resistance increase of this ITO film with the periodic submicron patterning over multiple bending cycles. The superflexibility and durability of

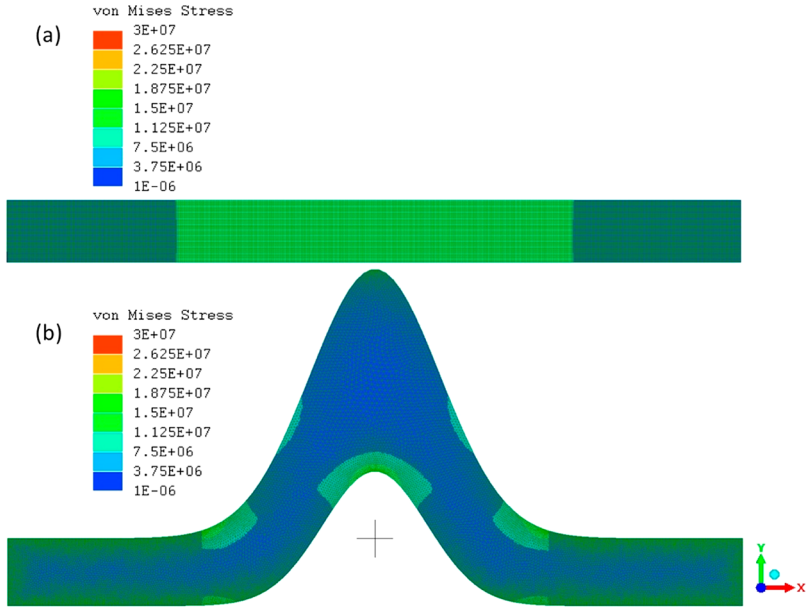

Figure 3. Tensile stress simulation of (a) continuous and (b) patterned ITO films with critical strain at 3.2 mm diameter of curvature. Stress in Pa units.

this ITO patterned PET substrate are evident by reaching 3.2 mm diameter of curvature and surviving after cycling for more than 50 times with a negligible resistance change. The total accumulated damage (resistance change/initial resistance) is only 3.2%. We found out the resistance change per cycle is a decaying as a function of the number of cycles; thus, in a conservative estimate utilizing the last resistance change measured between 40th and 50th cycles, we can offer an upper ceiling to the sheet resistance change for further cycles to be 0.025 Ω sq^{-1}/cycle. Given the small magnitude of this degradation rate, we can reasonably expect the film could keep performing over several hundreds to thousands of bending cycles without significant deterioration. The exact total of cycles it can live would naturally depend on the acceptable degradation of the particular application is being employed for.

How can such a simple structure make such a large difference? The reasons why the structure is successful in extending the bending capability of ITO can be appreciated by looking at finite element analysis of the stress in the film upon stretching. Figure 3 presents the von Mises stress map for both ITO pattern and flat film undergoing the strain imposed by bending to the 3.2 mm diameter of curvature. For reference, the critical stress and strain for cracking ITO are $\sigma_c = 5.8 \times 10^5$ Pa and $\varepsilon_c = 0.005$ (experimentally determined by standard tensile tests in conventional films). The local von Mises stress in the ITO pattern has a spatial distribution that clearly depends on the geometrical details of the structure, but it is lower than the critical stress of ITO at all points. In contrast, the stress in the flat film is quite uniform but surpassing σ_c. This indeed indicates that during the bending process the ITO pattern should survive at such small bending curvatures while the flat counterpart would never get there. In fact, the same simulation with strains produced under a 21 mm diameter curvature (the point that the continuous ITO film started to crack) on both of the continuous ITO film and ITO grating nanopattern (Figure S4) shows that indeed the flat sample should start to break around that strain level while the patterned ITO layer is far from it. All points of the generated stress map of the ITO patterned structure were much lower than σ_c, in full agreement with the experimental observations presented above. Focusing again on the patterned sample stress map when bent to 3.2 mm diameter of curvature, one can also note that the stress distribution presents some "hot-spots" at the bending "knees" of the pattern. The reason for those is that in the tensile mode the stretching is carried out by flexing those "knees" of the spring with a combination of local tensile and compressive stresses. The presence of compressive stress even when stretching the structure is fully benign, as the material does not strain beyond its capability, but hinges around those points, presumably limiting the opening of cracks. Simulations confirm that the larger the aspect ratio of the spring structure, the smaller the flexing needed to accommodate the substrate strain. Therefore, the potential for cracking is inverse to the structure aspect ratio.

In addition to the electrical conductivity and mechanical flexibility, high transparency is another important property that should be preserved and/or enhanced in the transparent conductive oxide films. To achieve better antireflective (AR) characteristics in the application of optoelectronic devices, a possible solution inspired from nature is the moth-eye antireflective scheme.[37−39] Eyes and wings of certain species of moth are covered in arrays of tapered pillars with a nanoscale period and height. Since the array features are on a length scale smaller than the wavelength of the incident light, the tapering of the pillars causes the incident photons to experience a gradual change in refractive index from that of the incident medium to that of the substrate. This is a well-known effect that has been employed earlier by others focused on improving ITO optical properties. Specific to our study, the fabrication of the ITO grating pattern at the right length scale and with a suitable periodicity for the optical matching creates a bonus-added moth-eye antireflector. Compared to the conventional flat commercial ITO film, the ITO grating patterned films exhibited a higher transmittance in most the visible and near-infrared spectrum range (500−900 nm) as shown in Figure 4a.

The 125 μm thick PET substrates used in this study present on their own an ∼80−90% transmittance in the visible and near-IR range. When normalized at this PET transmittance

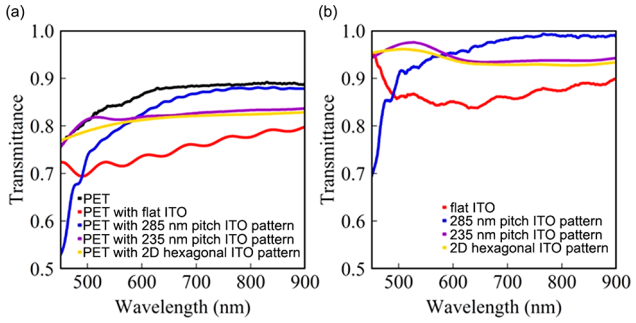

Figure 4. Comparison of (a) specular transmittance of ITO with PET substrate and (b) local transmittance of ITO only in the form of ITO continuous film and different ITO nanopattern.

(Figure 4b), the transmittance of ITO nanopattern alone is above 90% in the visible range and reaches 98% at red region wavelengths. In contrast, the normalized transmittance for flat commercial quality ITO film is around 85% in the whole visible range. The only disadvantage presented by the 285 nm period patterned samples is a pronounced transmittance decrease in the blue region (450–500 nm). The type of photoresist present in the structure contributes to some spurious blue light absorption, but this blue deficiency is primarily caused because the moth-eye effect does not reach those very short wavelengths. In fact, the dip in blue light transmission is associated with a large reflection enhancement, indicating constructive interference in the reflection optical channel. It is indeed worth noting that the AR characteristics are very sensitive to the periodicity of the pattern when its geometrical features are not significantly smaller than the wavelength of light. As the blue-light drop could be very detrimental in some applications, correction to this issue could be obtained by decreasing the grating period. This was confirmed by optical simulations (Figure S5), which predicts that when the periodicity of grating structure decreases to 235 nm the short wavelength optical impedance mismatch would shift to the UV region, disappearing accordingly of the visible range. Based on the simulation, an ITO periodic submicron grating structure with a periodicity of 235 nm was deposited on the PET substrates via the same methods mentioned before. This second set of gratings have a total height of 90 nm (which includes the grating height of photoresist and the thickness of ITO layer). As shown in Figure 4a, the optical transmittance of the ITO grating pattern with 235 nm pitch showed a great improvement in the blue wavelength region. The optical transmittance is >94% in the whole visible wavelength region (Figure 4b). It should be observed that compared to 285 nm pitch ITO nanopattern, the transmittance of 235 nm pitch ITO nanopattern ranging from 600 to 900 nm is ~5% lower. This near-IR drop is also predicted by the simulation shown in Figure S5. The analysis indicates that the transmission loss mainly arises from the reflection increase (no enhanced absorption), and both of them are connected with the sharpness of the high frequencies transmission dip.[40] During design simulations we noted this effect and in an ideal case, the transmission loss in blue wavelength region could be corrected without affecting the IR by decreasing only the pitch down to 190 nm without changing the pattern height. However, considering the required nanofabrication steps, such pitch and high aspect ratio were outside the dimensions we can reliably fabricate. Therefore, a trade-off between the decrease of the pitch and height was made to realize optimal transparency in the visible range scarifying a small amount of near-IR transmission.

We can expect that the lower aspect ratio of the 235 nm pitch samples was also going to affect their bending performance. Upon testing for 50 bending cycles, the total accumulated resistance change went up to 35% relative to the initial value, which is still outstanding relative to the flat control samples but relatively poor when compared to the 285 nm pitch ones. This lower aspect ratio (0.65) originated from limitations from the LIL step to create tall gratings with small pitch but also because the ITO film deposited was somewhat thicker (~90 nm as shown in Figure S6) than ideally designed (60 nm) for these particular set of substrates. It is easy to understand why these fabrication shortcomings were deleterious: the 235 nm samples turned out to be simply "flatter", and as the simulation work showed, the mechanical properties are truly continuous between the flat and grating structures, favoring better strain handling with larger grating aspect ratios. Nevertheless, the sheet resistance increased slowly after each tensile cycle, with the first cycle being the biggest single damaging event the film suffered. As the cycles accumulated, the resistance change per cycle became smaller, resulting from the 40th to 50th cycle in a 0.1Ω sq^{-1} sheet resistance increase per cycle. Importantly, although flatter, the smaller pitch samples showed no hint of the catastrophic failure typical of the flat control samples.

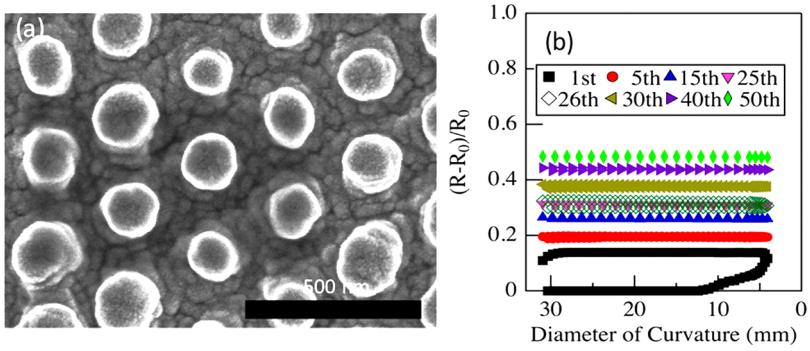

Figure 5. (a) SEM surface image of the morphology of the 2D ITO hexagonal nanopatterns on the surfaces of the polymer substrates. (b) Relative resistance increase of the 2D ITO hexagonal nanopatterns on the surfaces of the polymer substrates during the cycling bending test in two perpendicular directions. During each cycle, the minimum bending diameter of curvature was kept at 3.2 mm, and the specimen experienced 25 cycles of the reversible bending test for each direction.

All these 1D patterned ITO films can only be bended safely perpendicular to the grating lines. When bended along the grating lines direction, naturally the film behaves identical as a flat conventional film, cracking catastrophically at relatively large bending curvatures. For most commercial applications, multiaxis bending is certainly more broadly desired if not essential. Clearly what is required is a generalization of the 1D grating into a 2D pattern. A simple 2D square array is not satisfactory as in between the rows of hills and valleys, there is expected to find uninterrupted orthogonal domains of regular flat regions connected from end to end in the sample. We tested examples of such naive design, and their performance (not shown) was not superior to a regular flat film, suffering orders of magnitude resistance deterioration upon undergoing just one cycle in the bending test. A better approximation to the correct design is a 2D hexagonal nanopattern which does not present orthogonal flat domains. To realize it experimentally, the hexagonal array was fabricated by employing the LIL with a double exposure with the sample rotated 60° on its plane between exposures. Figure 5a shows the surface micrograph of the 2D hexagonal ITO periodic submicron grating structure deposited on the PET substrates. Figure 5b shows the relative resistance increase upon bending 25 cycles in two perpendicular directions successively. (The 26th cycle labeled in Figure 5b represents the first cycle for the second direction.) The accumulated relative resistance increase after 50 cycles was 48.4%. The higher relative resistance increase of this 2D ITO pattern was likely caused again by a somewhat lower aspect ratio mentioned above and also by the contribution of continuous flat regions between the pattern hills. However, the diminishing relative resistance change with the increase of the number of bending cycles was observed once again, with a rate of deterioration ~0.2 Ω sq^{-1}/cycle at the 50th bending test. By testing multiple samples, we randomized the alignment of the pattern relative to the axis of the bending instrument. The results showed small variations, but overall the flexibility and durability were independent of the bending directions in 2D. In other words, these mechanical properties were maintained no matter of the direction of the bending. In addition, given the small 235 nm pitch employed in the fabrication of this 2D sample, it also exhibited outstanding optical performance. The moth-eye effect described above effectively improved its transparency in the whole visible wavelength and made it comparable to that of the 1D grating patterned ITO structure fabricated with the same characteristic length as shown in Figure 4a,b.

4. CONCLUSION

In summary, we fabricated submicron 1D and 2D periodic grating patterns in ITO via a well-controlled laser interference lithography and sputtering deposition at room temperature. The optically transparent films retained requisite commercial level resistivity and sheet resistances in samples subjected to tight curvature bending down to 3.2 mm. Our observed properties surpass all the electrical resistance and resistivities previously reported for ITO formulations created to reach a high flexibility goal. Moreover, by controlling the periodicity of the ITO grating patterns, superflexible ITO film also exhibited significant light transmittance improvements. The success of a 2D hexagonal ITO nanopattern enabled multiaxial bending while maintained low resistance and high optical transparency. By employing both mechanical and optical simulations, the origin of the enhanced flexibility and transparency was revealed, suggesting a route to the ultimate 2D pattern with perfect performance in all the metrics of interests when subjected to multiaxial bending. These results clearly demonstrate a promising future for ITO in superflexible devices. The near perfect results of the 1D 285 nm grating pitch shows that improvements in 2D pattern requires a true generalization of the 1D effect. Admittedly, such perfection might come at a cost of complicating the nanopattern and nanofabrication. As the performance is simply geometry dependent, the graduation of the structural dimensions could tailor the optical and electrical performance depending on the application. For example, although not our initial intent, a controlled and known rate of resistance increase on bending cycle could give rise to other applications such as a bending counter to evaluate fatigue in a connected structural element, e.g., in aircraft structures. Uses of the patterned contacts could also bring additional design advantages for light extraction in light-emitting diodes or light trapping in solar cells.[41] Given the techniques employed here are all available for large areas and relatively high speed manufacturing, the potential for incorporating simple nanostructures in ITO and other transparent conductive oxides seems to be without inherent physical limitations. Notwithstanding these physical facts, the cost and viability at a commercial scale will depend on the cost of nanopatterning. In this work, we employed LIL, but newer approaches[42] such as nanoimprint or self-assembly might have a cost advantages in nanofabrication in a roll-to-roll production.

■ ASSOCIATED CONTENT

Supporting Information

The Supporting Information is available free of charge on the ACS Publications website at DOI: 10.1021/acsami.7b19098.

Scheme of fabrication of ITO periodic grating pattern with LIL process; SEM images of the continuous ITO film after reversible bending test; comparison of the SEM images of the ITO periodic grating patterns on the surfaces of the polymer substrates before and after cycling bending test; a tensile stress simulation of continuous and patterned ITO films with critical strain at 21 mm diameter of curvature; simulated transmittance spectra in ITO grating pattern with 285 nm of periodicity and grating with 235 nm of periodicity, respectively; a SEM cross-section image of the morphology of the ITO periodic grating patterns with 235 nm pitch on the surfaces of the polymer substrates (PDF)

■ AUTHOR INFORMATION

Corresponding Author

*E-mail rln@physics.unc.edu; Tel 1(919)962-7216 (R.L.).

ORCID

Rene Lopez: 0000-0001-6274-066X

Notes

The authors declare no competing financial interest.

■ ACKNOWLEDGMENTS

This research was funded through a grant provided by Eastman Chemical Company. We acknowledge in particular the contribution from Eastman California facility for the roll-to-roll sputtering deposition. The authors also thank Chapel Hill Analytical and Nanofabrication Laboratory (CHANL) and Dr.

Edward T. Samulki for their help at the different stages of this project.

REFERENCES

(1) Betz, U.; Kharrazi Olsson, M.; Marthy, J.; Escolá, M. F.; Atamny, F. Thin Films Engineering of Indium Tin Oxide: Large Area Flat Panel Displays Application. *Surf. Coat. Technol.* **2006**, *200*, 5751−5759.

(2) Park, S. K.; Han, J. I.; Kim, W. K.; Kwak, M. G. Deposition of Indium−tin-oxide Films on Polymer Substrates for Application in Plastic-based Flat Panel Displays. *Thin Solid Films* **2001**, *397*, 49−55.

(3) Kim, H.; Gilmore, H.; Piqué, A.; Horwitz, J. S.; Mattoussi, J. S.; Murata, H.; Kafafi, Z. H.; Chrisey, D. B. Electrical, Optical, and Structural Properties of Indium−tin−oxide Thin Films for Organic Light-emitting Devices. *J. Appl. Phys.* **1999**, *86*, 6451−6461.

(4) Kim, H.; Horwitz, J. S.; Kushto, G. P.; Kafafi, Z. H.; Chrisey, D. B. Indium Tin Oxide Thin Films Grown on Flexible Plastic Substrates by Pulsed-laser Deposition for Organic Light-emitting Diodes. *Appl. Phys. Lett.* **2001**, *79*, 284−286.

(5) Schmidt, H.; Flügge, H.; Winkler, T.; Bülow, T.; Riedl, T.; Kowalsky, W. Efficient Semitransparent Inverted Organic Solar Cells with Indium Tin Oxide Top Electrode. *Appl. Phys. Lett.* **2009**, *94*, 243302.

(6) Wang, Y.; Deng, J.; Di, J. J.; Tu, Y. Electrodeposition of Large Size Gold Nanoparticles on Indium Tin Oxide Glass and Application as Refractive Index Sensor. *Electrochem. Commun.* **2009**, *11*, 1034−1037.

(7) Wei, T. C.; Wan, C. C.; Wang, Y. Y.; Chen, C. M.; Shiu, H. S. Immobilization of Poly(N-vinyl-2-pyrrolidone)-Capped Platinum Nanoclusters on Indium−Tin Oxide Glass and Its Application in Dye-Sensitized Solar Cells. *J. Phys. Chem. C* **2007**, *111*, 4847−4853.

(8) Wu, H.; Hu, L.; Carney, T.; Ruan, Z.; Kong, D.; Yu, Z.; Yao, Y.; Cha, J. J.; Zhu, J.; Fan, S.; Cui, Y. Low Reflectivity and High Flexibility of Tin-Doped Indium Oxide Nanofiber Transparent Electrodes. *J. Am. Chem. Soc.* **2011**, *133*, 27−29.

(9) Yin, L. T.; Chou, J. C.; Chung, W. Y.; Sun, T. P.; Hsiung, S. K. Separate Structure Extended Gate H^+-ion Sensitive Field Effect Transistor on a Glass Substrate. *Sens. Actuators, B* **2000**, *71*, 106−111.

(10) So, S.; Choi, W.; Cheng, C.; Leung, L. M.; Kwong, C. F. F. Surface Preparation and Characterization of Indium Tin Oxide Substrates for Organic Electroluminescent Devices. *Appl. Phys. A: Mater. Sci. Process.* **1999**, *68*, 447−450.

(11) Nomura, K.; Ohta, H.; Ueda, K.; Kamiya, T.; Hirano, M.; Hosono, H. Thin-Film Transistor Fabricated in Single-Crystalline Transparent Oxide Semiconductor. *Science* **2003**, *300*, 1269−1272.

(12) Hecht, D. S.; Hu, L.; Irvin, G. Emerging Transparent Electrodes Based on Thin Films of Carbon Nanotubes, Graphene, and Metallic Nanostructures. *Adv. Mater.* **2011**, *23*, 1482−1513.

(13) Lu, H. T.; Yokoyama, M. Plasma Preparation on Indium-tin-oxide Anode Surface for Organic Light Emitting Diodes. *J. Cryst. Growth* **2004**, *260*, 186−190.

(14) Hu, L.; Hecht, D. S.; Grüner, G. Carbon Nanotube Thin Films: Fabrication, Properties, and Applications. *Chem. Rev.* **2010**, *110*, 5790−5844.

(15) Dan, B.; Irvin, G. C.; Pasquali, M. Continuous and Scalable Fabrication of Transparent Conducting Carbon Nanotube Films. *ACS Nano* **2009**, *3*, 835−843.

(16) Cao, Q.; Zhu, Z. T.; Lemaitre, M. G.; Xia, M. G.; Shim, M.; Rogers, J. A. Transparent Flexible Organic Thin-film Transistors That Use Printed Single-walled Carbon Nanotube Electrodes. *Appl. Phys. Lett.* **2006**, *88*, 113511.

(17) Wu, Z.; Chen, Z.; Du, X.; Logan, J. M.; Sippel, J.; Nikolou, M.; Kamaras, K.; Reynolds, J. R.; Tanner, D. B.; Hebard, A. F.; Rinzler, A. G. Transparent, Conductive Carbon Nanotube Films. *Science* **2004**, *305*, 1273−1276.

(18) Hu, L.; Hecht, D. S.; Grüner, G. Percolation in Transparent and Conducting Carbon Nanotube Networks. *Nano Lett.* **2004**, *4*, 2513−2517.

(19) Becerril, H. A.; Mao, J.; Liu, Z.; Stoltenberg, R. M.; Bao, Z.; Chen, Y. Evaluation of Solution-Processed Reduced Graphene Oxide Films as Transparent Conductors. *ACS Nano* **2008**, *2*, 463−470.

(20) Wu, J.; Becerril, H. A.; Bao, Z.; Liu, Z.; Chen, Y.; Peumans, P. Organic Solar Cells with Solution-Processed Graphene Transparent Electrodes. *Appl. Phys. Lett.* **2008**, *92*, 263302.

(21) Wang, X.; Zhi, L.; Müllen, K. Transparent, Conductive Graphene Electrodes for Dye-Sensitized Solar Cells. *Nano Lett.* **2008**, *8*, 323−327.

(22) Kuang, P.; Park, J. M.; Leung, W.; Mahadevapuram, R. C.; Nalwa, K. S.; Kim, T. G.; Chaudhary, S.; Ho, K. M.; Constant, K. A New Architecture for Transparent Electrodes: Relieving the Trade-Off Between Electrical Conductivity and Optical Transmittance. *Adv. Mater.* **2011**, *23*, 2469−2473.

(23) De, S.; Higgins, T. M.; Lyons, P. E.; Doherty, E. M.; Nirmalraj, P. N.; Blau, W. J.; Boland, J. J.; Coleman, J. N. Silver Nanowire Networks as Flexible, Transparent, Conducting Films: Extremely High DC to Optical Conductivity Ratios. *ACS Nano* **2009**, *3*, 1767−1774.

(24) Lee, J. Y.; Connor, S. T.; Cui, Y.; Peumans, P. Solution-Processed Metal Nanowire Mesh Transparent Electrodes. *Nano Lett.* **2008**, *8*, 689−692.

(25) Hu, L.; Kim, H. S.; Lee, J.; Peumans, P.; Cui, Y. Scalable Coating and Properties of Transparent, Flexible, Silver Nanowire Electrodes. *ACS Nano* **2010**, *4*, 2955−2963.

(26) Hong, W.; Xu, Y.; Lu, G.; Li, C.; Shi, G. Transparent Graphene/PEDOT−PSS Composite Films as Counter Electrodes of Dye-Sensitized Solar Cells. *Electrochem. Commun.* **2008**, *10*, 1555−1558.

(27) Tung, V. C.; Allen, M. J.; Yang, Y.; Kaner, R. B. High-throughput solution processing of large-scale graphene. *Nat. Nanotechnol.* **2009**, *4*, 25−29.

(28) Tung, V. C.; Chen, L. M.; Allen, M. J.; Wassei, J. K.; Nelson, K.; Kaner, R. B.; Yang, Y. Low-Temperature Solution Processing of Graphene−Carbon Nanotube Hybrid Materials for High-Performance Transparent Conductors. *Nano Lett.* **2009**, *9*, 1949−1955.

(29) Puetz, J.; Al-Dahoudi, N.; Aegerter, M. A. Processing of Transparent Conducting Coatings Made With Redispersible Crystalline Nanoparticles. *Adv. Eng. Mater.* **2004**, *6*, 733−737.

(30) Puetz, J.; Aegerter, M. A. Direct Gravure Printing of Indium Tin Oxide Nanoparticle Patterns on Polymer Foils. *Thin Solid Films* **2008**, *516*, 4495−4501.

(31) Heusing, S.; de Oliveira, P. W.; Kraker, E.; Haase, A.; Palfinger, C.; Veith, M. Wet Chemical Deposited ITO Coatings on Flexible Substrates for Organic Photodiodes. *Thin Solid Films* **2009**, *518*, 1164−1169.

(32) Maksimenko, I.; Wellmann, P. Low Temperature Processing of Hybrid Nanoparticulate Indium Tin Oxide (ITO) Polymer Layers and Application in Large Scale Lighting Devices. *Thin Solid Films* **2011**, *519*, 5744−5747.

(33) Yun, J.; Park, Y. H.; Bae, T. S.; Lee, S.; Lee, G. H. Fabrication of a Completely Transparent and Highly Flexible ITO Nanoparticle Electrode at Room Temperature. *ACS Appl. Mater. Interfaces* **2013**, *5*, 164−172.

(34) Alford, T. L.; Feldman, L. C.; Mayer, J. W. *Fundamentals of Nanoscale Film Analysis*; Springer: 2007; pp 1−336.

(35) Xie, Q.; Hong, M. H.; Tan, H. L.; Chen, G. X.; Shi, L. P.; Chong, T. C. Fabrication of Nanostructures with Laser Interference Lithography. *J. Alloys Compd.* **2008**, *449*, 261−264.

(36) Hinsberg, W.; Houle, F. A.; Hoffnagle, J.; Sanchez, M.; Wallraff, G.; Morri-son, M. Deep-Ultraviolet Interferometric Lithography as a Tool for Assessment of Chemically Amplified Photoresist Performance. *J. Vac. Sci. Technol., B: Microelectron. Process. Phenom.* **1998**, *16*, 3689−3694.

(37) Wilson, S. J.; Hutley, M. C. The Optical Properties of 'Moth Eye' Antireflection Surfaces. *Opt. Acta* **1982**, *29*, 993−1009.

(38) Sun, C. H.; Jiang, P.; Jiang, B. Broadband Moth-Eye Antireflection Coatings on Silicon. *Appl. Phys. Lett.* **2008**, *92*, 061112−1−061112−3.

(39) Boden, S. A.; Bagnall, D. M. Optimization of Moth-Eye Antireflection Schemes for Silicon Solar Cells. *Prog. Photovoltaics* **2010**, *18*, 195−203.
(40) Tikhodeev, S. G.; Yablonskii, A. L.; Muljarov, E. A.; Gippius, N. A.; Ishihara, T. Quasiguided Modes and Optical Properties of Photonic Crystal Slabs. *Phys. Rev. B: Condens. Matter Mater. Phys.* **2002**, *66*, 1−17.
(41) Fu, Y.; Dinku, A. G.; Hara, Y.; Miller, C. W.; Vrouwenvelder, K. T.; Lopez, R. Modeling Photovoltaic Performance in Periodic Patterned Colloidal Quantum Dot Solar Cells. *Opt. Express* **2015**, *23*, 779−790.
(42) del Campo, A.; Arzt, E. *Generating Micro- and Nanopatterns on Polymeric Materials*; Wiley-VCH Verlag GmbH & Co.: 2011; pp 27−41.